



**AIAA-2001-2142**

**AN EXPERIMENTAL EFFORT ON THE  
CONNECTION OF TURBULENCE STRUCTURES TO  
FAR-FIELD ACOUSTIC RADIATION IN A MACH 1.3  
JET**

**James Hileman, Brian Thurow, and Mo Samimy**

**THE OHIO STATE UNIVERSITY  
Department of Mechanical Engineering  
Columbus, OH 43210**

**7<sup>th</sup> AIAA/CEAS Aeroacoustics Conference  
May 28-30, 2001/ Maastricht, The Netherlands**

# AN EXPERIMENTAL EFFORT ON THE CONNECTION OF TURBULENCE STRUCTURES TO FAR-FIELD ACOUSTIC RADIATION IN A MACH 1.3 JET

J. Hileman<sup>1</sup>, B. Thurow<sup>1</sup>, and M. Samimy<sup>2</sup>  
 Department of Mechanical Engineering  
 The Ohio State University  
 Columbus, Ohio 43210

This work is part of an on-going effort to relate outstanding features of the far-field acoustic signature of ideally expanded, high speed, high Reynolds number jets to the dynamic interactions of large-scale structures within the jet mixing layer. It is believed that such information is essential and that it will lead to a better understanding of how turbulent mixing noise is created in high-speed jets. This, in turn, will lead to better modeling and control techniques. The characteristics of large amplitude far-field sound pressure events are examined via conditional sampling of the acoustic time signature. Based upon these results it appears that the large amplitude temporal events have distinct waveforms that collectively are responsible for the overall statistical properties of the acoustic radiation at 30°. An analysis of the sound data taken above and below the jet reveals that sometimes sound waves reach both sets of microphones with equal amplitude and no phase shift, and at other times there is attenuation and/or phase shift. Furthermore, there are also periods of relative quiet simultaneously recorded both above and below the jet. This would indicate that there are periods of asymmetric or axisymmetric, intense noise generation, and at other times there is no intense noise generation within the jet. As an example, the roll-up of a large structure is examined as a noise generation mechanism. Two cases are presented, one where the structure roll-up is in the top half of the mixing layer, and another where it is in the bottom half. It appears that structure roll-up in the top half of the mixing layer leads to the production of an intense sound wave that reaches an array above the jet. However, the roll-up of the structure below the jet centerline does not register as an intense noise source on the array above the jet. Our current and previous results have identified three mechanisms of noise generation: intense cross mixing layer interaction, tearing of large structures, and the roll-up of large structures.

## Introduction

Exhaust noise during aircraft takeoff continues to be a limiting factor in the growth of air traffic in the world. Unless means of reducing exhaust noise are found, airports will become more congested due to limits on new runway construction, while people living near airports will have their standard of living reduced if any airport expansion does occur. The exhaust noise from a typical jet engine is created by the turbulent mixing between the high-speed fluid of the jet engine and the ambient air surrounding the engine. Many of the average properties of jet engine noise are well known, but the underlying mechanism responsible for its creation is not. The end goal of this research effort is to determine how turbulence structures create mixing noise in ideally expanded, high-speed jets.

This study is an attempt to establish a correlation between the large coherent structures within the jet mixing layer and the measured noise in the

acoustic far-field. This is commonly known as establishing a causality correlation. In an unconventional manner, the acoustic data is examined in the time domain, and is only taken to the frequency domain as necessary when comparisons between individual dynamic features and the overall properties of the jet are desired. The jet in this study has a Mach number of 1.3, a Reynolds number in excess of  $10^6$ , and an exit diameter of 1 inch (this dimension will be referred to as a jet nozzle diameter,  $D$ , in much of this work).

The importance of large-scale structures to jet noise has been well known for about thirty years.<sup>1</sup> A large-scale structure within the jet shear layer has an average convective velocity,  $u_c$ , and a convective Mach number,  $M_c$ .<sup>2,3</sup> The convective velocity is important to this study because it is used to determine the location of noise emitting events during flow visualization. Theoretical formulas given in references 2 and 3 predict values of 206 m/s and 0.6, respectively for the convective velocity and Mach number. The actual

<sup>1</sup> Graduate student, member AIAA

<sup>2</sup> Professor, Associate Fellow AIAA

Copyright © 2001 by James I. Hileman. Published by the American Institute of Aeronautics and Astronautics, Inc. with permission.

convective velocity of the large-scale structures has been found to substantially deviate from the theoretical value. In an empirical study of coaxial Mach 1.5 jets, Murakami and Papamoschou<sup>4</sup> found an empirical model for the convective velocity. Using their relations, the average convective velocity of a Mach 1.3 jet without co-flow is approximately 311 m/s. The detailed experimental results of Thurow et al.,<sup>5</sup> obtained in the same jet facility as the current work using real-time flow visualizations, indicate that the convective velocity is much higher than the theoretical value but lower than the value predicted by the empirical model. While Thurow et al.<sup>5</sup> are in the process of refining their results, the convective velocity will be assumed as 300 m/s for this study.

For subsonic or ideally expanded supersonic jets, the dominant noise source is expected to originate from a mechanism that involves the turbulence structures within the mixing layer. If the convective velocity of the large-scale structures is subsonic, then this component of jet noise is commonly referred to as turbulent mixing noise. However, if the convective velocity is supersonic relative to the ambient, then the large-scale structures will emit Mach wave radiation. Since the convective Mach number for the jet in this study is subsonic, Mach wave radiation should be insignificant, and as such the focus will be on turbulent mixing noise.

Turbulent mixing noise is highly directional within the acoustic far-field. The noise emission is greatest at angles close to the downstream jet centerline. The preferred angle has been measured to vary from 25° to 45° with respect to the downstream jet axis.<sup>6</sup> The majority of the turbulent mixing noise production emanates from a region that includes the end of the potential core.<sup>6-9</sup> Morrison and McLaughlin<sup>7</sup> found that the dominant noise production mechanism for three low Reynolds number jets (Mach numbers of 1.4, 2.1, and 2.5) is the rapid growth, saturation, and decay of instability waves near the end of the potential core. They conjectured that the majority of the noise is due to the rapid decay (disintegration) of the instability waves, and this disintegration involves a “relatively violent fluid dynamic action.” In studies of low speed jets and mixing layers, the noise creation process has been linked to vortex pairing.<sup>10-12</sup> Sarohia and Massier<sup>13</sup> performed experiments with high-speed schlieren motion pictures that were synchronized with near-field pressure measurements. They studied excited subsonic jets with Mach numbers ranging from 0.1 to 0.9 with a Reynolds number of approximately  $10^6$ . They found that large instantaneous pressure pulses were formed whenever two large-scale structures merged; however, the passage of a large structure did not significantly change the near-field pressure signal.

## Previous work

The current work is part of an on-going research effort to relate the flow structure to the acoustic field of a Mach 1.3 jet.<sup>14-17</sup> Previous results are summarized in this section. The jet has a potential core length of about 6 jet diameters, and a preferential noise emission direction of 30° at a peak frequency of approximately 3 kHz, ( $St_D = 0.2$ ). Both symmetric and asymmetric interactions of turbulence structures within the mixing layer of the jet were observed in single- and double-pulse flow visualizations. A time analysis of the acoustic signal revealed that there are individual noise events, grouped periodic noise events, and long periods of time without any large amplitude noise production events.<sup>17</sup>

The individual peak noise events have similarities to the crackle phenomenon first documented by Ffowcs Williams et al.<sup>18</sup> They used the skewness of the sound data as a measure of crackle. If the skewness was less than 0.3, then the jet was not considered to be crackling, while a jet with skewness in excess of 0.4 was crackling distinctly. The skewness for this jet is under 0.1, which is well below the criteria set by Ffowcs Williams et al.<sup>18</sup> Thus, as was expected because of the low Mach number of the jet, these large amplitude events are not considered to be crackle by the given definition. This is consistent with the work of Ffowcs Williams et al., as they found a similar Mach number jet did not crackle. The periodic peak events consisted of several individual peaks that oscillated between compression and expansion with every peak possessing a magnitude that is above some defined threshold. The frequency content of these events was very similar to the overall acoustic far-field of the jet. Many of the short periodic segments had peak frequencies between 2 and 5 kHz, and were comprised of between 3 and 8 oscillating positive and negative peaks. The acoustic field of the jet also possessed relatively quiet periods of time that could last well over 1 ms. The criterion for relative quiet was established as periods of time where there were no sound pressure peaks in excess of 1.5 times the standard deviation,  $\sigma$ . A statistical analysis of temporal noise data revealed that the jet is producing large amplitude noise events, exceeding twice its standard deviation, over 25.6 percent of the time, while the jet was in relatively quiet modes, enduring at least 0.38 ms, 21.4 percent of the time.<sup>17</sup>

Much of the previous work has focused on relating the flow structure of the jet to far-field noise using flow imaging and either a two- or four-microphone array. The dual-microphone array was used with double-pulse laser illumination and two digital cameras.<sup>14,15,17</sup> The four-microphone array was utilized with real-time flow visualization via a pulse

burst laser and high frame rate camera.<sup>16</sup> Unfortunately, the retarded time formula used in references 14, 15, and 16 was incorrect; therefore, the locations of the noise emitting region of the jet during laser illumination were incorrect in those references. The correct formula is  $d_{LF} = d - u_c t_L$  and it is properly defined in reference 17. The noise source temporal locations given in reference 15 have been corrected and implemented in reference 17. The correction of this error led to a definite improvement in the correlation between flow structure and noise emission. These corrected results showed that interactions between large structures across the jet mixing layer and ‘tearing’ of large-scale structures are two likely mechanisms of intense noise production.<sup>17</sup> Reference 17 and the corrected version of reference 16 are posted on the web at: <http://rclsg.eng.ohio-state.edu/~samimy/index.html>

**Experimental Arrangement**

*Anechoic Chamber and Jet Facility*

All of the experiments were conducted in the optically accessed anechoic chamber of the Gas Dynamics and Turbulence Laboratory (GDTL) at The Ohio State University. This facility allows for the measurement of jet flow via advanced optical diagnostics in an anechoic environment. Details of the chamber and flow facilities can be found in previous publications.<sup>14-17,19</sup> The 1 inch exit diameter, Mach 1.3 nozzle was designed using the method of characteristics. The actual Mach number of the nozzle was measured as 1.28 and the Reynolds number was  $1.08 \times 10^6$ . A schematic of the experimental arrangement as viewed from above is shown in Figure 1. Some of the items in the schematic will be described in detail below.

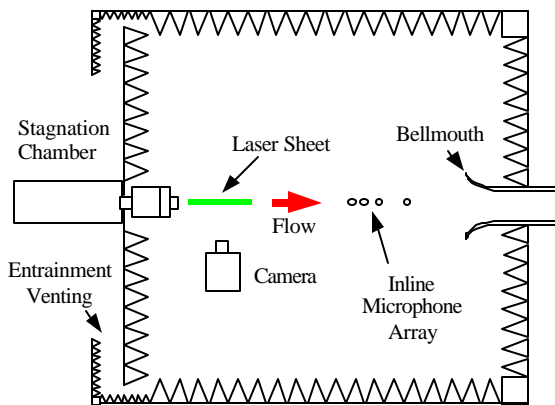


Figure 1: Schematic of the anechoic chamber as seen from above with simultaneous experimental equipment shown.

*Inline Microphone Array - Instantaneous Source Location*

A novel approach in microphone array design was used for these experiments. Since the goal of this research is to relate the acoustic far-field of the jet to its dynamic flow structure, the origin of individual sound waves needs to be determined. This was accomplished by measuring the amount of time it takes a sound wave to pass two microphones at known locations. The array was located at an angle of  $30^\circ$  to capture the noise generating phenomena that are responsible for the large amplitude, low frequency spectral peak that is typically associated with the largest structures within the flow. The array was comprised of four, quarter inch microphones (three B&K 4135, and one B&K 4139) that were separated by 1.5, 2.0, and 2.5 inches. The array is shown in the schematic of Figure 2.

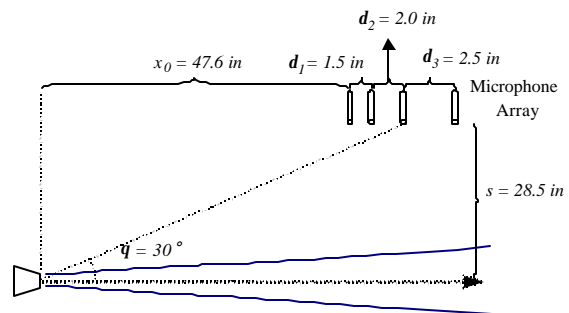


Figure 2: Schematic of the inline microphone array.

All of the items within the chamber were covered in half-inch thick acoustic foam to minimize the potential acoustic reflection. The sound data were acquired at a rate of 1 million samples per channel per second. This large acquisition rate was chosen to maximize the accuracy in measuring the time separation. The data reduction procedure for a two-microphone array is described in detail in reference 17, while its application to the four-microphone array is described in more detail in reference 16. Some details are given below.

The separation between when a sound wave reached any two different microphones, along with information of the geometry of the array with respect to the jet exit, was used to determine where the sound wave had originated. The time separation was computed using the cross-correlation of the two microphones signals. A 0.35 ms segment from the front microphone that contained the sound peak of interest at its center was chosen and then equally long segments from the second microphone signal were examined to determine the maximum cross-correlation. The source location technique was simplified by assuming that the noise originated on the centerline of the jet. Since there were four microphones, there were six time separations and six different calculations for

any sound wave that reached the microphone array. These six source locations were then averaged to determine the noise source location used in the present work. Any of the six locations that were less than  $-5 D$  or greater than  $25 D$  were considered spurious and were not included in the average. The accuracy of the array was checked with a simple air blower, and the actual location of the air blower was in good agreement with the computed location.<sup>16</sup> Further, the vertical location of the air blower was varied to determine its effect on the predicted streamwise location of the noise source.

To relate noise emission to large structures that were captured within flow visualization images, one has to be able to relate the time of noise emission to the time when the flow structure was captured by the visualization. Rarely will the laser illuminate the flow while an interaction between structures is producing a sound wave. What is far more likely is that the laser will illuminate an interaction either before or after it has produced a sound wave. Therefore, one needs to measure the time lag between the flow visualization and the emission of the sound wave by the noise source. Details on how this was done can be found in references 16 and 17. This calculation relies on convective velocity, and as discussed in the introduction, a value of 300 m/s will be used for these calculations.

#### Dual Floor and Ceiling Arrays - Directivity Assessment

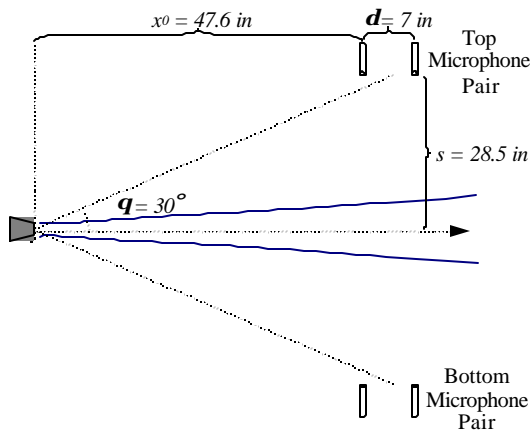


Figure 3: Schematic of the microphone arrays that were mounted from the ceiling and floor to ascertain the directivity of acoustic emission.

In addition to the in-line array mounted from the ceiling, an additional array was created to study the instantaneous azimuthal variation of the far-field turbulent mixing noise. Two microphones were mounted from the ceiling with a 7 inch separation, and two additional microphones were mounted from the floor with the same relative configuration (the sideline and streamwise locations as well as the separation were matched). Figure 3 shows a schematic of the array

setup. By examining the time traces of the sound pressure from these two array sets, an attempt was made to determine how the potential azimuthal variation of far-field acoustic radiation directivity and the gross effect of refraction would influence the interpretation of our results. The equipment and techniques used to analyze data from this array were the same as that used for the inline array except there was only one pair of microphones on each side of the jet.

#### Real-Time Flow Visualization

The flow was visualized via illumination of condensed water particles within the jet mixing layer. The warm, moist air of the ambient is entrained into the cold, dry air that is exiting the jet, thus forming the jet's mixing layer. Within the mixing layer, the moisture within the ambient air condenses into small particles that mark the majority of the mixing layer and its motion. The condensed particles within the mixing layer were illuminated with a pulse burst laser and then captured with an SMD camera. Both systems are capable of operating at a MHz rate. However, the camera was limited to seventeen frames, and as such, the flow was visualized over this time with either a 5  $\mu$ sec or 10  $\mu$ sec delay between consecutive images (laser pulses). This fast laser/camera system as well as the techniques used to condition the raw images are described in depth in Thurow et al.<sup>5,20</sup> The laser was located outside of the anechoic chamber and the beam from the laser was redirected into the chamber through a 2.5 cm hole in one of the large structural beams of the chamber. A frame structure connected to the ceiling of the chamber held the optics that were used to create the laser sheet. The optics framework was covered with acoustic foam to minimize acoustic reflection. The laser sheet passed through the jet centerline in the streamwise direction. The SMD camera was placed inside of the chamber, perpendicular to the laser sheet, and it captured the flow from 4.5  $D$  to 10.5  $D$ . The camera and optics within the chamber were covered in half-inch thick acoustic foam to minimize potential acoustic reflection.

## Results and Discussion

#### Average Properties of Large Amplitude Sound Pressure Events

All of the sound pressure peaks that were in excess of  $2\sigma$  were ensemble averaged to determine the average properties of the large amplitude peaks. This was accomplished by taking one millisecond of data before and after every peak exceeding  $2\sigma$ , phase aligning the peaks, and then ensemble averaging these data segments. The time corresponding to the

maximum amplitude, which is the common reference point for all of the peaks, was determined by recording the maximum value of the pressure signal between crossing zero heading toward a peak (either positive or negative), and returning to zero after the peak. This process of finding peaks and then ensemble averaging the individual waveforms was performed separately for the positive peaks (501 events) and negative peaks (486 events) to get the two average waveforms that are shown, respectively, in Figures 4 and 5.

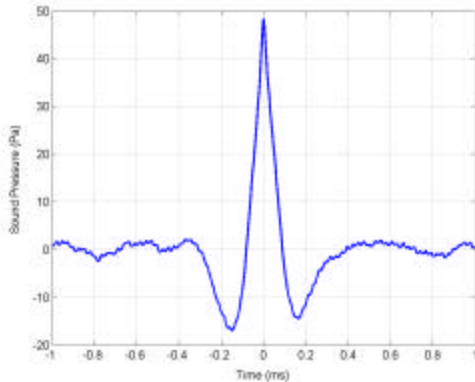


Figure 4: Average positive large amplitude sound pressure waveform.

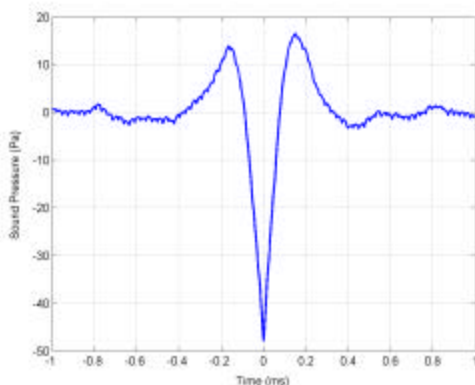


Figure 5: Average negative large amplitude sound pressure waveform.

The shapes of the waveforms are quite remarkable because they have sharp, distinct peaks with side lobes. Except for minor differences in the side lobes, the two waveforms are near mirror images of each other with the mirror plane being the abscissa. In both, the central peak reaches an absolute maximum of nearly 50 Pa, while the side lobes have absolute values of about 14 and 16 Pa. As a check for the validity of the waveforms in Figures 4 and 5, several randomly chosen positive waveforms have been plotted together in Figure 6. As expected, the figure bares many similarities to Figure 4. In both, the large central positive peak has negative peaks on either side. The majority of pressure measurements around -0.2 ms

(before the central peak) are negative (between 0 and -40 Pa), while those around 0.2 ms (after the peak) change sign (between 20 and -40 Pa). This would explain the difference in magnitude of the side lobes. It would appear that expansions before compressions occur more regularly than expansions after the compression, although the reasons for this are not yet clear.

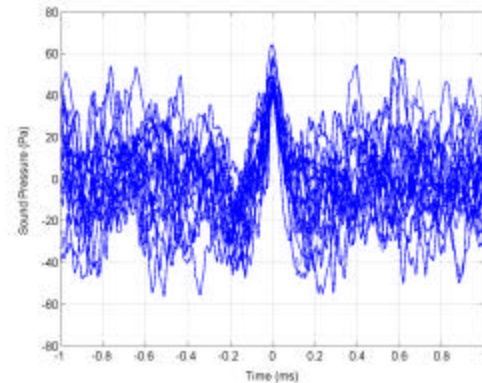


Figure 6: Twenty individual waveforms that were used to create the average positive waveform of Figure 4.

A similar analysis was performed for a threshold level of  $1.5\sigma$ . This yielded about 1200 positive and 1200 negative peaks. Those results showed similar trends to the  $2\sigma$  threshold results, and as such, will not be presented here. The peaks of the average waveforms were about 40 Pa, and the side lobes had equal absolute magnitudes of about 13 dB. Based on these results, it would seem that the asymmetry in the side lobes are a result of the stronger interaction in the flow that result in the largest amplitude far-field acoustic radiation.

The central part of the positive and negative  $1.5\sigma$  average waveforms (-0.5 to 0.5 ms) were transformed to the frequency domain and converted to power spectral density plots. These spectra are given in Figure 7 along with the overall spectrum for 250 sets of sound data taken in 6 ms blocks at a rate of 1 MHz (3.0 seconds of total sound data). The spectra have a remarkable similarity. The magnitudes of the three curves are nearly identical between 1 and 4 kHz, while the two average waveform spectra roll off more rapidly at higher frequencies. The average waveform spectra were not plotted below 1 kHz as their spectra only have a frequency resolution of 1 kHz ( $10^6$  acquisition rate / 1000 samples). The spectra for the  $2\sigma$  threshold waveforms are nearly identical in shape to those given in Figure 7 with an increase in amplitude of about 2 dB.

The amazing match of the spectra between 1 and 4 kHz shows how well these average waveforms are capturing the overall noise character of the jet at the  $30^\circ$  observation angle. This has tremendous

consequences for understanding the correlation between turbulence structures and far-field acoustic, flow/acoustic control, and aeroacoustic modeling. Since the average waveform was created by averaging many individual large amplitude sound events, and the spectra from the average waveform accurately recreates the overall spectra for the jet, it would appear that the large amplitude sound events are in fact responsible for the generation of the intense low frequency sound that is observed at downstream angles.

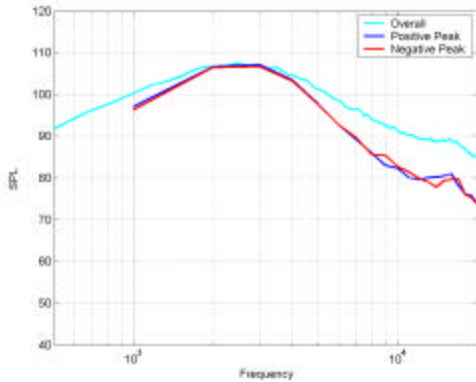


Figure 7: Overall spectrum with spectra for the average positive and negative large amplitude sound pressure waveforms.

As a means of understanding these large amplitude sound events, the absolute magnitude of each large event (in excess of  $1.5\sigma$ ) has been plotted in Figure 8 versus the location where the wave originated. A total of 2.5 seconds of data was used. Data points that had a standard deviation within the six individual location measurements, using the four microphones, in excess of 2D were not included, thus leaving 4199 data points to be plotted in the figure. The scatter plot does not have any events with magnitude under 29 Pa as these are below the  $1.5\sigma$  threshold. The largest amplitude sound waves are emanating from the region between 5 and 12 D. The number of all events drops off considerably after 12D. Figure 9 shows a histogram of noise emission locations. The same criteria used to create Figure 8 are used here as well. The mean of the noise source origins is 8.0 D, and the standard deviation is 3.0 D. Figure 9 is similar to a plot presented in reference 16. In this set of noise source locations, sound origins between  $-5$  and 25 D are accepted (the algorithm used in ref. 16 only accepted values between 0 and 20 D). Thus, histogram has a similar shape to the one given in reference 16; however, the edges trail off more gradually since the boundaries on the noise source location algorithm exceed the range of actual noise origins. The vast majority (77 %) of the noise sources come from the region between 5 and 11 D. It would thus appear that not only are more large amplitude

noise events occurring between 5 and 11 D, but this is also the area where the most intense noise is generated.

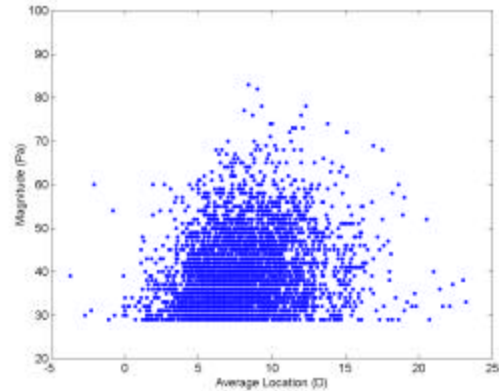


Figure 8: Absolute magnitude of sound pressure peaks versus downstream origin of the sound wave (amplitudes in excess of  $1.5\sigma$ ).

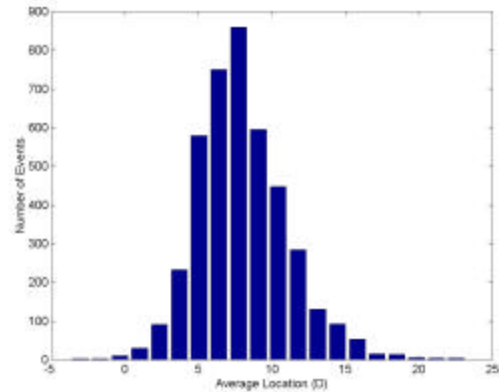


Figure 9: Histogram of origin location of large amplitude sound waves (amplitude larger than  $1.5\sigma$ ).

*Average “Noisy” and “Relatively Quiet” Real-time Movies*

The unconditional average image of the jet (average of randomly selected images) as well as the average image during periods of large amplitude noise production and relative quiet can be readily obtained since the locations of noise production during the flow visualizations are known. The random average of the jet was created by ensemble averaging the seventh flow image from 77 random flow visualization sets. This overall average image is shown in Figure 10 (flow is from left to right with the streamwise distance marked on the figure in D). The bright areas are the two sides of the mixing layer, while the dark area at the center is the unmixed core of the jet. Frames from each flow visualization set that had captured a noise event in the process of creating a large sound peak in excess of  $2\sigma$  were also ensemble averaged. This data set consisted of 36 images. The requirements on the relative quiet

images were that the quiet period be longer than 0.76 ms and that it contain the time 3.7 ms, which is the average time when a large amplitude sound wave that was captured within a flow image would have reached the microphone. The fifth image from each flow visualization movie that had acoustic signatures matching these requirements was also ensemble averaged (29 images in all). To eliminate the problems caused by differences in shot-to-shot intensity variations, prior to averaging each of the images was normalized so its maximum intensity would be one.

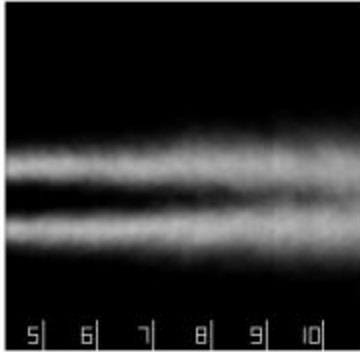


Figure 10: Average image of the jet. The average was created from 77 random flow movies.

Figure 11 shows the intensity of each of the three average images (“noisy,” “relatively quiet,” and “random”) at select downstream locations. Upstream of 7D, the three curves have nearly identical centerline intensity. However, downstream of 8D, the “noisy” image has the largest centerline intensity, thus showing the presence of very large-scale structures, responsible for bringing the ambient air to the center, and hence more interaction between the two sides of the mixing layer. This is not surprising as cross mixing layer interaction was speculated as a cause of large amplitude noise production in references 16 and 17.

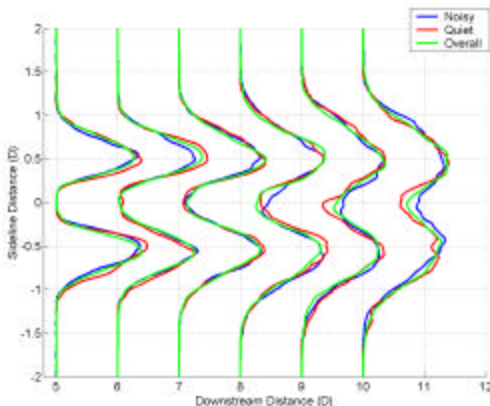


Figure 11: Plots of the average intensity for the noisy, relatively quiet, and overall images for various downstream locations.

These observations are further supported by the flow image of Figure 12, which shows the average

“relatively quiet” flow image subtracted from the average “noisy” flow image. The figure is a grayscale image with distance from the nozzle exit (in jet diameters) given beside the tic marks. In the figure, the intensity is maximum along the centerline downstream of 8D, thus indicating the “noisy” flow images had larger structures and thus there was more interaction within the jet.

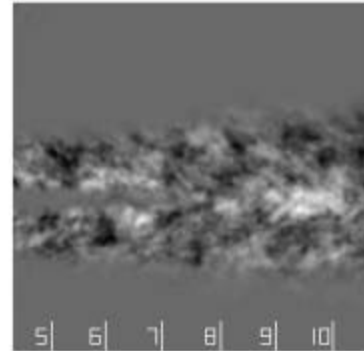


Figure 12: Average “noisy” image minus the average “relatively quiet” image.

*Directivity/Refraction Effects*

In all of the work presented so far, the microphone array was located on one side of the jet. A fundamental question that needs to be addressed is whether the array was registering any acoustic radiation generated on the opposite side of the jet due to a combined refraction and directivity effect. The refraction would be caused by the variations in density and speed of sound across the mixing layer, while the intensity directivity of any noise mechanism within the jet is not well known. The directivity is probably not uniform around the jet centerline, as asymmetric turbulence structures are often observed. The floor and ceiling arrays were used to explore these effects.

Figures 13 and 14 show time signatures of the microphone data from the front microphone in the top array and the front microphone in the bottom array. One of the interesting features of Figure 13 is the relatively quiet time period between 18 and 19 ms. Both of the microphones are recording relatively quiet sound pressures during this time period. This would likely be caused by a lack of significant noise generation mechanisms of any kind within the jet.

Another interesting repeating occurrence is exhibited in Figure 13. The first positive pressure peak (it has a small circle above it) from the top microphone has a much larger intensity than the corresponding peak from the bottom microphone. Figure 14 has further examples of this phenomenon, which have all been marked with small circles. It appears that there is an attenuation of the sound wave between the top and bottom directions. This attenuation could be caused if

the sound originated from one side of the mixing layer. Any sound waves that were created by such a source that is located within one side of the mixing layer would have to travel through the opposite side of the mixing layer to get to the microphone array that is on the opposing side of the anechoic chamber. During its propagation, the sound wave would likely have attenuation and/or changes in its direction due to the effects of refraction.

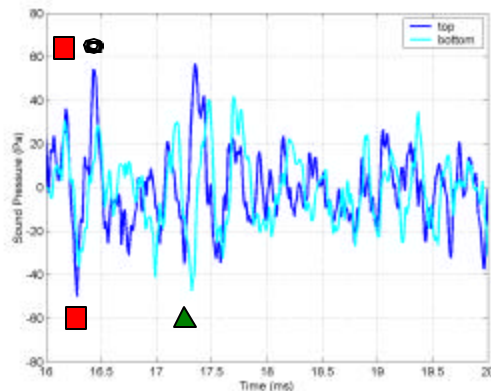


Figure 13: Microphone data that show a period of relative quiet as heard both above and below the jet. Symbols for this and Figure 14: circles – attenuation, triangles – phase shift, squares – minimal attenuation and phase shift.

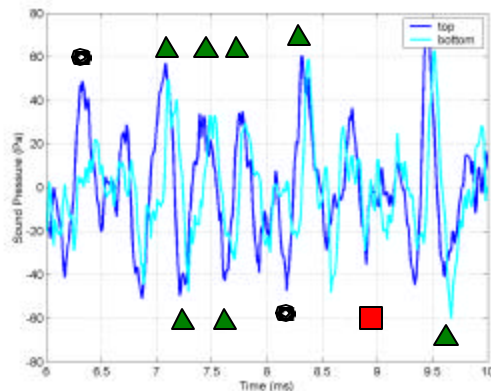


Figure 14: Microphone data that show various effects on sound propagation as measured both above and below the jet.

The change in direction, which would be caused by refraction, would lead to a phase shift between when the sound wave reached the two sets of microphones. This type of event is clearly observed once in Figure 13 and several times in Figure 14. Sound peaks that have an identifiable phase shift have been marked with triangles. The phase shift is not large, but it does exist between sets of top and bottom microphone peaks. There are other sets of peaks in Figures 13 and 14 that have a minimal (possibly zero)

phase shift, and these events have been marked with squares. Axisymmetric sound waves that originate from the jet centerline should experience equal refraction/attenuation from both sides of the mixing layer, and as such should reach both sets of microphones at the same with equal magnitude.

Based on these results, there are three observed phenomena: uniform quiet, uniform phase and amplitude, and directional changes to phase and amplitude. These phenomena would likely indicate that during certain periods of time the jet has a general lack of noise generation, sometimes the noise generation is axisymmetric, and at other times, the noise generation is asymmetric. Furthermore, an array mounted on one side of the jet is not going to give an accurate portrayal of all of the noise generation mechanisms within the jet; it might have recorded an attenuated, phase shifted wave which would not accurately describe the noise source. Therefore, flow interactions that are within the mixing layer that is closest to the microphone array will be considered as the sources of intense noise generation. This element of the experiment technique will be examined in greater detail in subsequent studies.

#### *Simultaneous Measurements*

This section will present two sets of flow visualization images that were taken with simultaneous microphone array measurements. Each flow visualization “movie” consists of a set of 16 images separated by 10  $\mu$ sec. The flow is from left to right, and the tic marks at the bottom of the image are in jet diameters from the jet exit. The flow images have two plots below them. The first is a spectrogram of the sound data. It was created by determining the power spectrum for 1000 data points sections (the data was acquired at a rate of  $10^6$  samples per second) for sections that overlap each other by 750 data. Below the spectrogram is a sound pressure time trace for the front and rear microphones of the array.

During the time when the images in Figure 15 were taken, the jet was in a period of relative quiet from 3 ms to past 4.5 ms, as is seen in the time signature of Figure 16. The spectrogram of this time trace shows the low intensity of the low frequency noise during this period of relative quiet (compare it to the region between 2 and 2.5 ms). Through analysis of the array acoustic data, it was determined that no noise events in excess of  $1.5 \sigma$  were produced during this movie. The quiet period, using the aforementioned definition, is 1.6 ms long, during which a large-scale structure would travel about 18 nozzle exit diameter. This period of quiet is quite remarkable considering the large roll-up of successive large structures within the bottom of the mixing layer (in image 13, the structures are centered at 7 D and 9 D; image numbers are 1 to 16, from left to right, top to bottom). The structure at 9 D in image 13

formed by the mixing layer first becoming wavy in appearance (frames 4-6 between 7 D and 9D), and then rolling into a large, round structure (frames 8-14 between 8 D and 9 D). This process is very much like that described by instability wave theory.<sup>6,7</sup> The upstream structure (at 7 D in image 13) forms between 5 and 7 D over the course of the movie by several structures combining and rolling up together. There were additional cases, not shown here, of large structure roll-up within the bottom half of the mixing layer occurring without large amplitude sound waves reaching the ceiling mounted microphone array.

How is it possible that the microphone array did not record any sound from these large structure roll-ups? There are three possible explanations. First, structure “roll-up” might not be a mechanism of intense sound generation; second, the sound waves did not reach the microphones due to attenuation/refraction within the upper mixing layer; or finally, the noise generated by the roll-up of large structures has a non-uniform directivity pattern. In the non-uniform noise generation scenario, the roll-up would have created intense sound that traveled in a variety of directions, but one of the directions it did not travel was the location of the microphone array. The next data set should help to answer this question.

The flow visualization movie in Figure 17 shows the roll-up of a very large structure within the top half of the mixing layer. The structure is centered at 8 D within image 7. The time signature of Figure 18 has a large sound pressure compression (positive pressure peak) that is marked with a small circle. The spectrogram of the acoustic data is presented for comparison to that of Figure 16, which had a long section of relative quiet and low amplitude at low frequency. This spectrogram is more typical. The origin of the marked peak was estimated as 7.3 D (this is marked by a solid square in all the images of Figure 17), and it was created 100  $\mu$ s after the first image of the movie, which is 50  $\mu$ s before the last image was taken. The standard deviation in the six individual noise source locations was 1.2 D. Assuming a convection velocity of 300 m/s, a large structure at 5.9 D in the first frame would be at 7.3 D during noise emission; this same structure (assuming a constant convection velocity) would be located at 7.9 D in the last image. The location of such a hypothetical convecting structure has been marked in the images by an open square. The sound wave was created when the two squares line up. By examining the roll-up process in the flow images, one can see the open square lags the large, developing structure by about one jet diameter. This should be expected since the structure is above the jet centerline. If the noise origin were 0.5 D above the centerline, then the actual noise emission location would be 0.8 D further downstream. Thus, there is very

good agreement between the origin of the marked large peak and the large structure. The roll-up of structures was also determined to be the mechanism of sound generation in a large number of other data sets. One such set is presented in the revised version of reference 16. Therefore, the large roll-up of the structure in the bottom half of the mixing layer of Figure 16 likely created a large amplitude sound wave. However, due to the attenuation/refraction of the sound wave within the upper mixing layer and/or the possibility that this type of noise generation mechanism would create a highly directional noise pattern, a sound wave did not travel toward the location of the array. Further insight into the physics of structure roll-ups, as well as additional flow movies, is available in reference 5.

### Summary of Results

This work presents some interesting findings about the average properties of the large amplitude sound pressure peaks. These results were obtained via conditional sampling of the sound peaks, examination of the average origin of sound production, and consideration of the average condition of the jet during sound production as opposed to periods of relative quiet. The potential effects of directivity / refraction were explored with two sets of microphones, one above the jet, the other below. Then these directivity considerations were applied to the interpretation of the roll-up of large structures as a source of intense sound generation.

The properties of positive and negative large amplitude sound pressure events were examined via conditional sampling of two millisecond long segments of the acoustic time signature. When ensemble averaged, the peaks collapse into distinct waveforms with a sharp, central peak and two side lobes. These waveforms have frequency content that accurately represents the overall statistical properties of the acoustic radiation at 30°. This has tremendous consequences for understanding the correlation between turbulence structures and the far-field acoustics, flow/acoustic control, and aeroacoustic modeling. The average origin for all of the large amplitude sound waves was examined via a scatter plot of the amplitude versus origin as well as a histogram of the sound origin. The vast majority (77%) of sound production occurs between 5 and 11 D. Further, the majority of the largest amplitude sound waves originate from this region of the jet.

Images taken of the jet during noise production and during periods of relative quiet were respectively averaged and then compared to random data. The average image taken during noise generation has a higher intensity along the jet centerline than the other two cases. This indicates the existence of large-

scale structures in the intense noise generation cases that entrain the ambient air into the center of the jet and thus stronger interaction. This observation gives further credence to the claims in references 16 and 17 that cross mixing layer interaction generates intense sound waves.

A preliminary study of the instantaneous directivity of the jet was presented. Three different phenomena were observed. Sometimes both the top and bottom mounted arrays recorded relatively quiet periods as would be expected if there were no noise generation within the jet. Further, the large amplitude sound pressure events were often much more intense in one direction than the other, or the two sound peaks had a phase shift. Either of these could be due to the asymmetry of the noise source with respect to the jet centerline or asymmetry in the emitted acoustic directivity. Finally, there were times when both microphone arrays recorded the same magnitude for the large amplitude sound events. This would result if the sound wave was produced by a symmetrically radiating noise source near the jet centerline where the effects of propagation through the mixing layer would be the same in both directions.

The array did not identify the roll-up of structures within the bottom half of the mixing layer as a noise generator, but it did locate a roll-up within the top half of the mixing layer as a noise generator. It would seem that this type of interaction in the bottom half of the mixing layer creates intense noise, but this noise does not reach the microphones that are above the jet. This could be due to the other side of the mixing layer either attenuating the sound pressure intensity or refracting the sound pressure waves away from the array; or it could be due to an asymmetric acoustic directivity of the noise source. Based upon this and previous studies, there are three identified mechanisms of noise generation: intense cross mixing layer interaction,<sup>16,17</sup> tearing of large structures,<sup>17</sup> and the roll-up of large structures.<sup>16</sup>

The movies that were presented in this paper can be viewed at our web site as well as further examples of the various noise generation mechanisms that were presented here. In addition, references 5, 16-17, 19, and 20 can be downloaded in pdf format from the web site. The GDTL web site address is:

<http://rclsgl.eng.ohio-state.edu/~samimy/index.html>

### Acknowledgment

This work is sponsored by the Air Force Office of Scientific Research with Dr. Steve Walker as the Technical Monitor. The first author would like to thank the Ohio Space Grant Consortium for his doctoral fellowship. The authors would like to thank Satish

Narayanan of UTRC and Tom Barber of the University of Connecticut for all of their help in developing the microphone techniques used in this work as well as our stimulating conversations in the field of turbulence noise generation.

### References

1. Crow, S.C., and Champagne, F.H., "Orderly Structure in Jet Turbulence," *J. Fluid Mechanics*, Vol. 48, Part 3, 1971, pp. 547-591.
2. Bogdanoff, D.W., "Compressibility Effects in Turbulent Shear Layers," *AIAA J.*, Vol. 21, No. 6, 1983, pp. 926-927.
3. Papamoschou, D. and Roshko, A., "The Compressible Turbulent Mixing Layer: An Experimental Study," *J. Fluid Mechanics*, Vol. 197, 1988, pp. 453-477.
4. Murakami, E. and Papamoschou, D., "Eddy Convection in Coaxial Supersonic Jets," *AIAAJ*, Vol. 38, No. 4, 2000, pp. 628-635.
5. Thurow, B., Hileman, J., Samimy, M., and Lempert, W., "An in-depth Investigation of Large-scale Structure Evolution in a High-speed Axisymmetric Jet," AIAA Paper 2001-0148, 39<sup>th</sup> AIAA Aerospace Sciences Meeting and Exhibit, Reno, NV, January 2001.
6. Tam, C.K.W., "Jet Noise Generated by Large-Scale Coherent Motion." *Aeroacoustics of Flight Vehicles: Theory and Practice*. Vol. 1, edited by H.H. Hubbard, 1991, pp. 311-390.
7. Morrison, G.L, and McLaughlin, D.K., "Noise Generation by Instabilities in Low Reynolds Number Supersonic Jets," *J. Sound and Vibration*, Vol. 65, 1979, pp. 177-191.
8. Yu, J.C., and Dosanjh, D.S., "Noise Field of a Supersonic Mach 1.5 Cold Model Jet," *J. of the Acoustical Society of America*, Vol. 51, No. 5, Pt. 1, 1972, pp. 1400-1410.
9. Schaffar, M., "Direct Measurements of the Correlation Between Axial in-jet Velocity Fluctuations and Far-field Noise near the Axis of a Cold Jet," *J. Sound and Vibration*, Vol. 64, No. 1, 1979, pp. 73-83.
10. Kibens, V., "Discrete Noise Spectrum Generated by an Acoustically Excited Jet," *AIAA J.*, Vol. 18, April 1980, pp. 434-441.
11. Colonius, T., Lele, S., Moin, P., "Sound Generation in a Mixing Layer," *J. Fluid Mechanics*, Vol. 330, August 1997, pp. 375-409
12. Mitchell, B., Lele, S., Moin, P., "Direct Computation of the Sound Generated by Vortex Pairing in an Axisymmetric Jet," *J. Fluid Mechanics*, Vol. 383, October 1998, pp. 113-142.
13. Sarohia, V., and Massier, P.F., "Experimental Results of Large-scale Structures in Jet Flows and

- Their Relation to Jet Noise Production,” AIAA Paper 77-1350, AIAA 4<sup>th</sup> Aeroacoustics Conference, Atlanta, GA, October 1977.
14. Hileman, James I., Identification of Noise Sources in a Mach 1.3 Axisymmetric Jet via Simultaneous Flow and Noise Measurement, Masters Thesis, The Ohio State University, Department of Mechanical Engineering, 2000.
  15. Hileman, J. and Samimy, M., “An Attempt to Identify Noise Generating Turbulent Structures in a High-speed Axisymmetric Jet,” AIAA Paper 2000-2020, 6<sup>th</sup> AIAA/CEAS Aeroacoustics Conference, Lahaina, HI, June 2000.
  16. Hileman, J., Thurow, B., and Samimy, M., “Determination of Noise Sources within a high-speed Jet via Simultaneous Acoustic Measurements and real-time Flow Visualization,” AIAA Paper 2001-0374, 39<sup>th</sup> AIAA Aerospace Sciences Meeting and Exhibit, Reno, NV, January 2001.
  17. Hileman, J. and Samimy, M., “On Turbulence Structures and the Acoustic Far-Field of a Mach 1.3 Jet,” to appear in 2001 *AIAA J.*
  18. Ffowcs-Williams, J.E., Simson, J., and Virchis, V.J., “Crackle’: an annoying component of jet noise,” *J. Fluid Mechanics*, Vol. 71, Part 2, 1975, pp. 251-271.
  19. Kerechanin C.W., Samimy, M., and Kim, J.-H., “Effects of Nozzle Trailing Edge Modifications on Noise Radiation in a Supersonic Rectangular Jet,” AIAA paper 2000-0086, 38th AIAA Aerospace Sciences Meeting and Exhibit, Reno, NV, January 2000.
  20. Thurow, B., Lempert, W., and Samimy, M., “MHz Rate Imaging of Large-Scale Structures within a High-Speed Axisymmetric Jet,” AIAA Paper 2000-0659, 38<sup>th</sup> AIAA Aerospace Sciences Meeting and Exhibit, Reno, NV, January 2001.

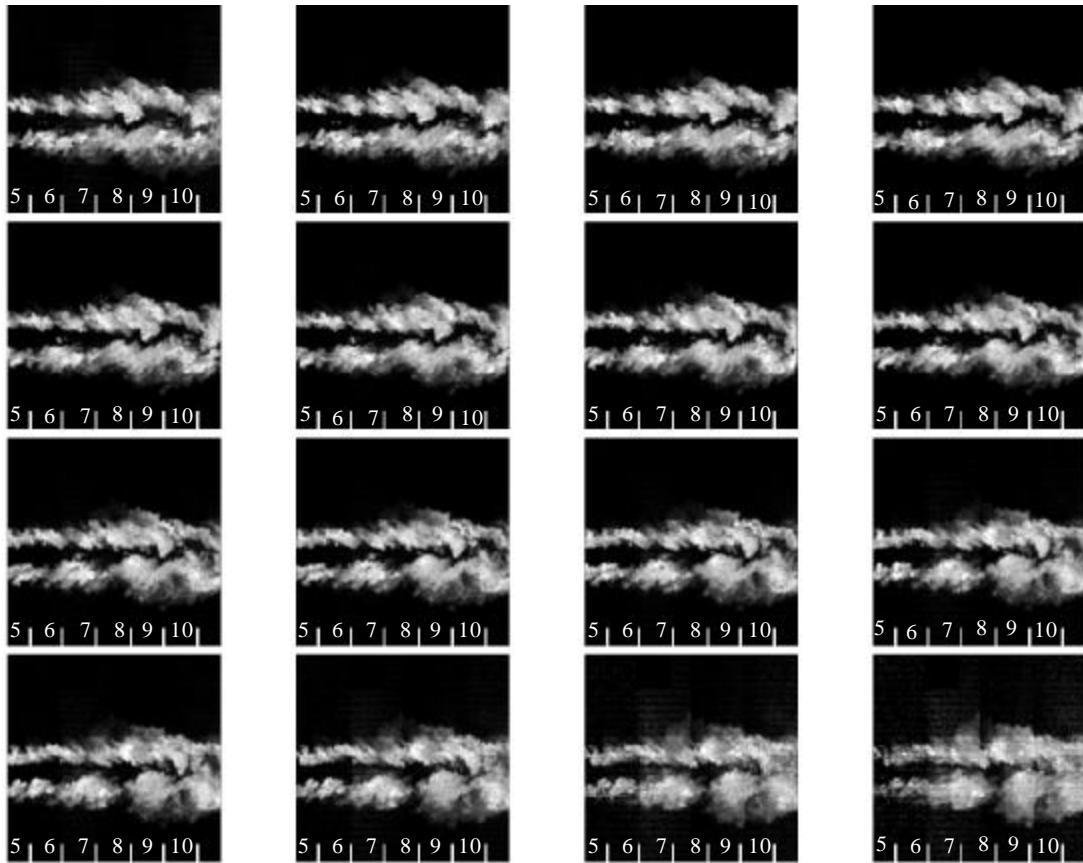


Figure 15: Flow visualization set showing the rolling up of large structures within the bottom half of the mixing layer. The images are separated by 10  $\mu$ sec, and the flow is from left to right.

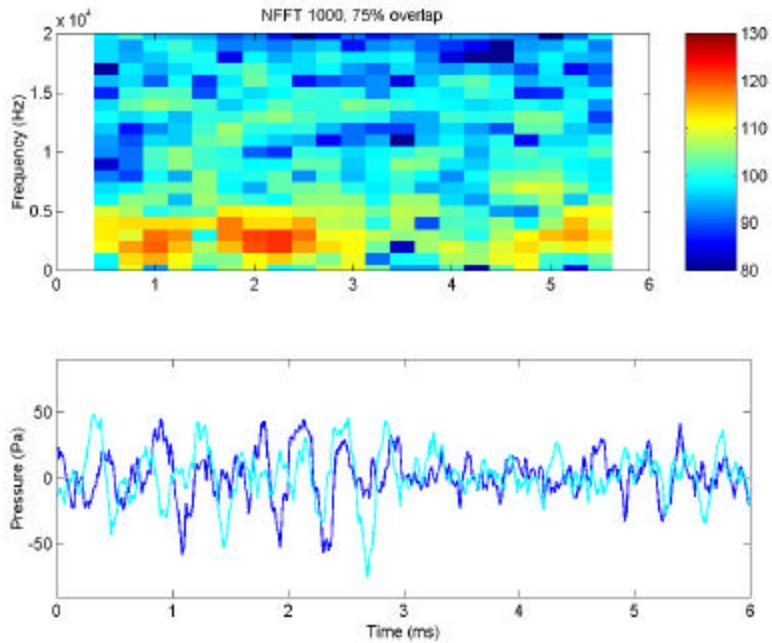


Figure 16: Time signature and spectrogram of the microphone array data taken simultaneously with the flow images of Figure 15, spectrogram units are in dB.

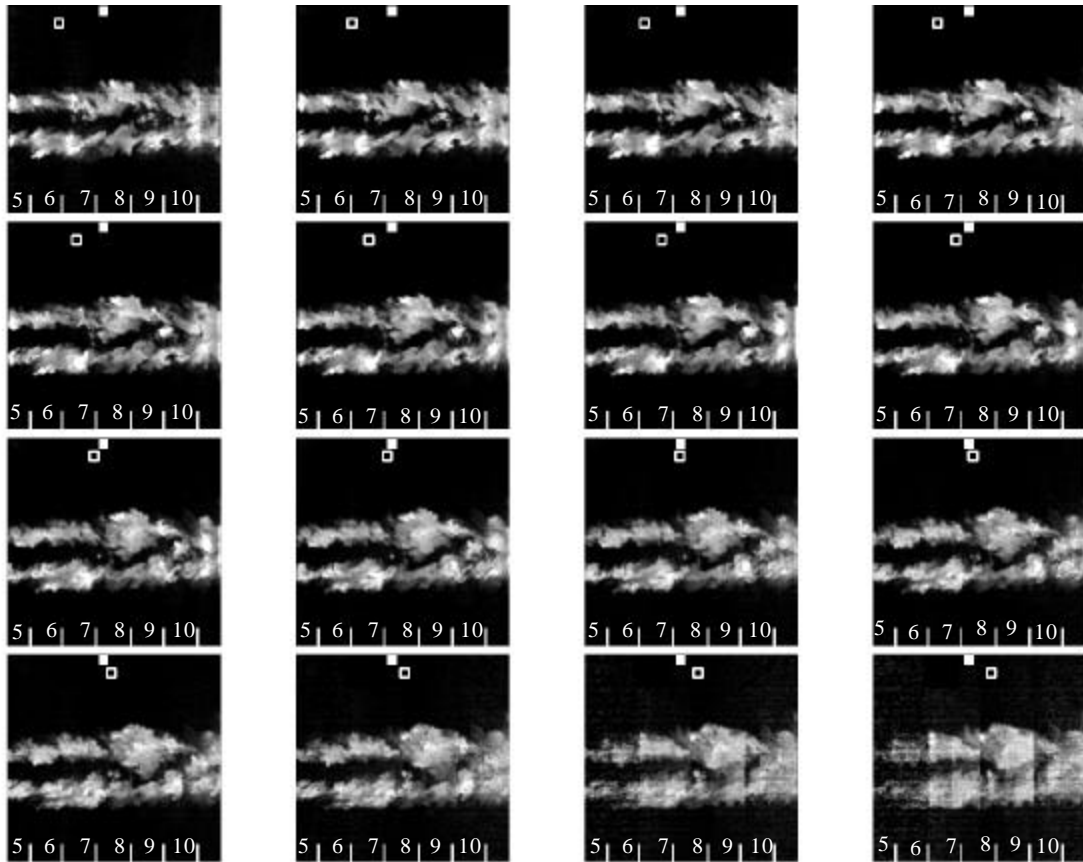


Figure 17: Flow visualization set showing the rolling up of a large structure within the top half of the mixing layer. The images are separated by 10  $\mu$ sec, and the flow is from left to right. The squares show the location of noise emission (filled), and where this portion of the jet was during each image (open).

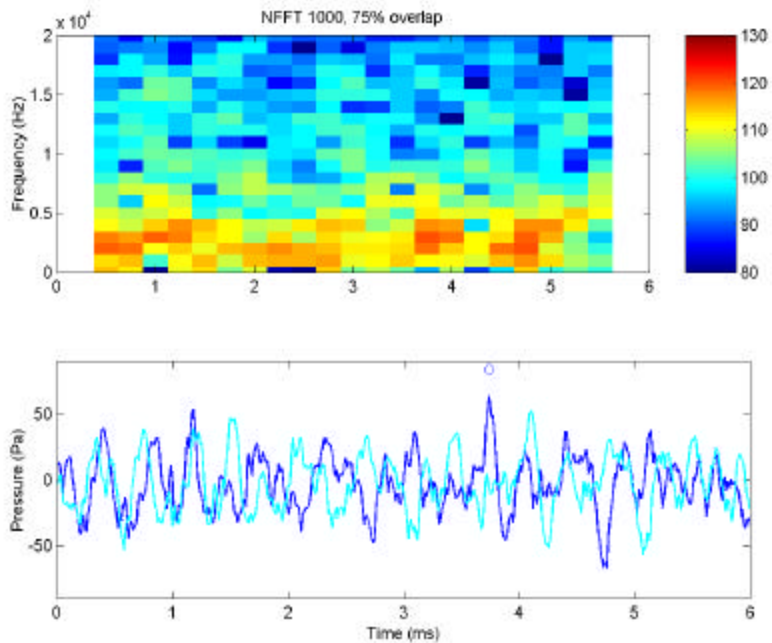


Figure 18: Time signature and spectrogram of the microphone array data taken simultaneously with the flow images of Figure 17, spectrogram units are in dB.